Simultaneously Improved Efficiency and Stability in All-Polymer Solar Cells by a P-i-N Architecture

Yalong Xu,[1] Jianyu Yuan,[1] Shuyan Liang,[2] Jing-De Chen,[1] Yuxin Xia,[3] Bryon W. Larson,[4] Yusheng Wang,[1] Gregory M. Su,[5] Yannan Zhang,[1] Chaohua Cui,[6] Ming Wang,[7] Haibin Zhao,[2] Wanli Ma[1]**

[1]Institute of Functional Nano & Soft Materials (FUNSOM), Jiangsu Key Laboratory for Carbon-Based Functional Materials and Devices, Joint International Research Laboratory of Carbon-Based Functional Materials and Devices, Soochow University, Suzhou, 215123, P. R. China

[2]Shanghai Ultra-precision Optical Manufacturing Engineering Research Center and Key Laboratory of Micro and Nano Photonic Structures (Ministry of Education), Department of Optical Science and Engineering, Fudan University, Shanghai, 200433, P. R. China

[3]Biomolecular and Organic Electronics, IFM, Linköping University, SE-58183 Linköping, Sweden.

[4]Chemistry & Nanoscience Center, National Renewable Energy Laboratory, Golden, Colorado 80401, United States

[5]Advanced Light Source, Lawrence Berkeley National Laboratory, Berkeley, California 94720, United States

[6]Laboratory of Advanced Optoelectronic Materials, College of Chemistry, Chemical Engineering and Materials Science, Soochow University, Suzhou 215123, China.

[7]Center for Advanced Low-Dimension Materials, State Key Laboratory for Modification of Chemical Fibers and Polymer Materials, Donghua University, Shanghai 201620, China.

Corresponding Author: jyyuan@suda.edu.cn (J. Y.); wlma@suda.edu.cn(W. Ma).

ABSTRACT

All-polymer organic solar cells offer exceptional stability. Unfortunately, the use of bulk heterojunction (BHJ) structure has the intrinsic challenge to control the side-chain entanglement and backbone orientation to achieve sophisticated phase separation in all-polymer blend. Here, we revealed that the P-i-N structure can outperform the BHJ ones with a nearly 50% efficiency improvement, reaching a power conversion efficiency approaching 10%. This P-i-N structure can also provide enhanced internal electric field and remarkably stable morphology under harsh thermal stress. We have further demonstrated generality of the P-i-N structure in several other all-polymer systems. Considering the adjustable polymer molecular weight and solubility, the P-i-N device structure can be more beneficial for all-polymer systems. With the design of more crystalline polymers, the antiquated P-i-N structure can further show its strength in all-polymer system by simplified morphology control and improved carrier extraction, becoming a more favorite device structure than dominant BHJ structure.

TOC GRAPHICS

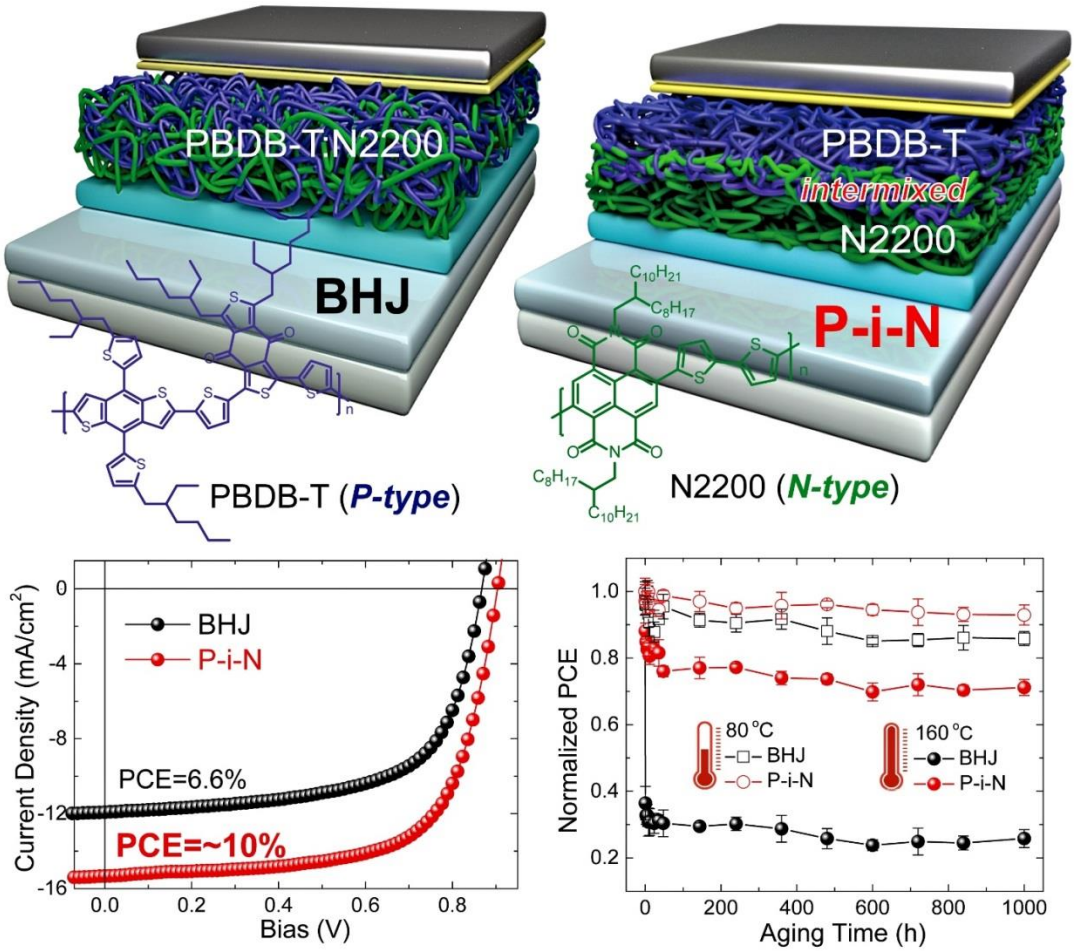

Conjugated polymer materials offer immense tunability in their molecular structure, optical bandgap, energetic position of the electronic states, and less toxicity with scale-up synthesis compared to emerging metal halide perovskite materials.[1-4] Additionally, polymeric materials exhibit efficient charge transport and high absorption coefficient across a broad range of the solar spectrum,[5-6] which led to the first report of 10% organic solar cells.[7] Quite recently, it has been shown that organic nonfullerene acceptors can further extend the solar cell response spectrum,[8-10] and power conversion efficiencies (PCEs) above 15% have been demonstrated in these systems.[11] During the past few years, we and few other groups have developed efficient polymer-polymer (all-polymer) solar cells.[12-17] With this polymer-polymer combination,[18] the active layer exhibits outstanding thermal and mechanical device stability.[19] We have also shown that all-polymer solar cell devices are less sensitive to thermal stress, D/A composition and processing environment relative to the polymer-fullerene and polymer-molecule ones.[20] Although all-polymer solar cells come with many advantages, their performance has been limited by low short-circuit current density (J_{sc}) and low fill factor (FF).[21-24] A general explanation is that convectional fullerene acceptors are spherically symmetric materials which can have close contact with the donor polymers in arbitrary directions to achieve efficient charge transfer.[25-26] Similarly, nonfullerene molecular acceptors tend to form highly crystalline domains with long-range charge delocalization that lowers the Coulomb barrier and hence improves exciton dissociation. However, the similar properties between donor and acceptor polymers increase the difficulty to optimize the polymer/polymer interfaces to achieve preferable contact and molecular orientation. We have indicated that reduced polymer ordering and unfavorable orientation at polymer/polymer interfaces leads to limited charge delocalization, inefficient carrier transport and larger potential

barrier, which can reasonably explain the origin of the lower J_{sc} and FF in all-polymer devices.[27]

In a solution-processed organic photovoltaic device, the organic/organic interfacial properties are extremely important in deciding the solar-to-electricity conversion efficiencies, as well as device long-term stability.[28] In 1995, Heeger *et al.* first reported significantly enhanced power conversion efficiency (PCE) *via* a network of internal polymer-soluble fullerene derivative bulk heterojunction (BHJ),[1] which benefits from efficient photo-to-exciton generation process. During the past two decades, the BHJ structure dominated research on solution-processed organic solar cells.[29] However; the electronic structure at the interface could strongly depend on how the materials make contact with each other, which in turn is affected by many factors such as materials crystallinity, processing condition etc. From the start of organic solar cells, C. W. Tang reported thermally evaporated two-layer structure organic solar cells with a PCE around 1%.[30] Photo-generated excitons dissociate into free charges at material interfaces driven by the energy offset, and the bilayer structure creates efficient charge transport pathways to the electrodes. Inspired by the early stage research of organic photovoltaic, we here demonstrated that the sequentially processed P-i-N junction structure could be extremely advantageous for all-polymer solar cells. It should be noted that the sequentially processed organic solar cells has been previous reported in both polymer-fullerene and polymer-polymer systems from quasi-orthogonal solvents, achieving more adjustable morphology compared to the BHJ ones.[31-33] However, the obtained best PCE from P-i-N structure is around 5%. During the preparation of the manuscript, efficient polymer-molecule nonfullerene solar cells using P-i-N structure have been reported,[34-35] which indicates increased attention on the P-i-N structure in organic photovoltaic. Efficient charge transfer and significantly improved charge transport

successfully take place across the polymer/polymer interfaces to achieve improved J_{sc} and FF relative to the conventional BHJ. An open-circuit voltage (V_{oc}) of 0.904 V, J_{sc} of 15.33 mA cm^{-2}, FF of 68.7% and PCE of 9.52% are obtained, outperforming the PCE of 6.58% in BHJ analogue cell. In the P-i-N device, a vertical phase separated morphology composed of highly ordered donor and acceptor domains with buried thin polymer-polymer BHJ is obtained from solution processing, where carrier dissociation and transport achieve an optimal balance to enhance charge collection at each electrode. Such P-i-N structure can fully utilize the advantages in absorption and carrier transport for single polymeric phase, and demonstrates promising potential for all-polymer devices.

Figure 1A-1B shows the chemical structures of the donor and acceptor polymers and device architecture of all-polymer solar cells in this work. The polymer PBDB-T and its derivatives are widely used electron donors in organic nonfullerene solar cells,[8] and n-type polymer N2200[36] (also known as P(NDI2OD-T2)) is popular electron acceptor in efficient all-polymer solar cells.[18] N2200 exhibits excellent electron transporting properties, but on the other hand, the relative high molecular weight and strong interaction between the polymer backbones decrease its solubility in common organic solvents.[37-38] The difference in solubility between donor and acceptor polymer allows us to sequentially deposit layer-by-layer structures. As shown in Figure S1 (Supporting Information, SI), without heating or stirring, N2200 has limited solubility in chloroform. Therefore, we fabricated the inverted BHJ (ITO/ZnO/PBDB-T:N2200/MoO_3/Ag) and P-i-N device architecture (ITO/ZnO/N2200/inter-mixed/PBDB-T/MoO_3/Ag) to compare the photovoltaic performance. The absorption of donor/acceptor polymers is well complemented to cover the whole visible to NIR region (300-850 nm, Figure S2). In order to avoid the effect of thickness on absorption, we compared the

absorption coefficient of both films, and it is quite interesting that the absorption of the P-i-N film is enhanced compared to the BHJ film. To investigate the influence of device architecture on light harvesting, we first simulated the spectral- and position-dependent optical field distribution in the BHJ and bilayer device respectively.[39] In **Figure 1C**, the region with strong optical field for BHJ film is beyond 780 nm, which, unfortunately, mismatch the absorption range of active film. For the P/N bilayer film (**Figure 1D**), the high intensity field covers a larger range from 650 nm to the infrared. Meanwhile, the optical field in the visible region is also enhanced. Basically, the additional interface between donor and acceptor affects the light interference in the BHJ device, which further results in the redistribution of electromagnetic field. As a result, the absorption of both PBDB-T and N2200 is increased, indicating improved exciton generation in P-i-N all-polymer devices. In addition, it is worth noting that the pure D/A polymer phase in P-i-N film has evidently higher crystallinity than that in BHJ film, which can also help to achieve higher optical absorption coefficient,[40] and the change of the film crystallinity will be investigated in the following part.

As shown in **Figure 2A** and **Table 1**, the PBDB-T:N2200 BHJ device shows a moderate efficiency of 6.37±0.21 %, similar to previous results.[41-42]. Quite recently, through adopting a modified conventional device structure, Yang et al. reported the efficient PBDB-T:N2200 BHJ device with a best PCE of 8.61%.[43] Fortunately, the strategy of P-i-N structure can take full advantages of both improved absorption and carrier transport in highly-crystalline pure N2200 phase. After optimization (see Table S1-S4, SI), a significantly enhanced average J_{sc} of 14.79 mA/cm^2, slightly improved V_{oc} of 0.898 V and FF of 66.3 % is observed, giving a remarkably improved average PCE of 9.28 % and the best one of 9.52%. As shown in **Figure 2B**, the optimal thickness of PBDB-T and N2200 is determined to be 50 nm and 60 nm, respectively.

The total optimal thickness of 110 nm is similar with that of the BHJ devices. When further increasing the thickness of either PBDB-T or N2200, the P-i-N all-polymer devices exhibit gradually decreased efficiency. Meanwhile, the dark $J-V$ characteristics in Figure S3 indicate better diode properties for P-i-N device, showing lower leakage current and ideality factor (For an ideal diode, the ideality factor is equal to 1). It is not surprising the P-i-N structure can outperform the popular BHJ structure in all-polymer system. The polymer blend has the intrinsic challenge to control the side-chain entanglement and backbone orientation between high molecular weight polymers with long chains. The strong inter- or intra-chain interactions make it extremely difficult to achieve sophisticated phase separation using conventional treatment like thermal annealing,[44] processing additive[45] etc. In contrast, the P-i-N structure can overcome the big challenge in control the polymer blend morphology. However, well control the intermixed region of D/A polymers is critical to achieve efficient charge separation. As shown in Table S1-S4, the inter-mixing region between the pure p-type and n-type polymers should be well manipulated to achieve optimal thickness and better contact with the bottom and upper layer.

The development of OPV has reached a stage where device stability should be further considered for entering commercial market. Previous report has demonstrated that the morphological change under thermal stress in BHJ film is one of the core issues limiting the OPV stability.[20] All-polymer blend devices have already been reported to exhibit improved thermal stability compared to PCBM and nonfullerene based BHJ devices. As shown in **Figure 2C**, we can observe both BHJ and P-i-N devices show steady PCE value under continuous thermal stresses at 80 ^{o}C. However, the P-i-N all-polymer devices still exhibit decent performance under continuous thermal stresses at a higher temperature of 160 ^{o}C for nearly 1000 hours, indicating exceptional stable morphology even under harsh environment. The universality

of P-i-N structure were also explored in other all-polymer systems based on popular donor polymer P3HT, PT8,[19] and J51[46] (see Figure 2D). As shown in Table S5 in SI, it is clear that all device parameter including V_{oc}, J_{sc} and FF are simultaneously enhanced in P-i-N devices in comparison with the conventional BHJ cells. All these results demonstrate that the P-i-N structure can be a universal strategy to overcome the intrinsic morphological issue in all-polymer BHJ structure and achieve stable and superior device performance.

To compare the number of generated charge carriers/number of excitons generated by photon absorption in BHJ and P-i-N, the external quantum efficiency (EQE) and the internal quantum efficiency (IQE) of optimized BHJ and P-i-N PBDB-T:N2200 devices have been measured, with the results shown in **Figure 3A**. We can observe an overall increase in EQE for P-i-N based device, indicating higher incident photon to converted carriers ratio in P-i-N based devices. the absorption (extracted from reflection spectrum (R) by 100%-R, Figure S4, SI) and, To clarify the origin of EQE enhancement, the IQE of both systems was also measured (the absorption of both devices was shown in Figure S4, SI).[27] Exclude the factor of absorption enhancement, we observe more evident increase of IQE value for P-i-N device, especially around the absorption peaks of N2200 at 400 nm and 730 nm, indicating largely increased photo-exciton contribution from the polymer acceptor. Note that N2200 usually contributes poorly to current in BHJ all-polymer solar cells, which has been generally thought to be an obstacle to achieve similar high J_{sc} value with the device based on small-molecule acceptor. In the P-i-N structure, the improved absorption may help to achieve more efficient charge generation, and modify vertical phase separation is beneficial for efficient charge transport and overcoming both charge recombination especially in the N2200 phase. The improved charge dynamic process,

which will be investigated in the following part, could explain the higher EQE and IQE in the P-i-N based devices.

To confirm the IQE results, we further conducted time-resolved microwave conductivity (TRMC) measurements.[47] TRMC is a contactless technique that probes local carrier mobility on the length scale of carrier delocalization, so the measured mobility is not as impacted by morphology, grain boundaries, or other problems that limit long range charge transport measurements in a device. Therefore, these measurements give an indication of the potential performance or upper limit that one should expect from a particular blend. As shown in **Figure 3B**, the TRMC figure of merit ($\phi\sum\mu$) measured during the experiment is a product of the quantum efficiency of free carrier generation per photon absorbed (ϕ) and the sum of the mobilities of electrons and holes ($\sum\mu$). The P-i-N PBDB-T: N2200 blend (0.20 $cm^2\ V^{-1}\ s^{-1}$) exhibits a higher yield-mobility product relative to the BHJ film (0.14 $cm^2\ V^{-1}\ s^{-1}$). Bi-exponential fits of the photoconductivity transient, as shown in Figure S5, reveal the average carrier lifetime is also longer in the P-i-N than BHJ (950 ns *vs.* 880 ns). We further compared the TRMC free carrier diffusion length according to the mobility and lifetime results for each blend. As shown in **Figure 3C**, the P-i-N PBDB-T:N2200 blend (D_L=844 nm) exhibits a higher free carrier diffusion length relative to the bulk device (D_L=709 nm). In comparison with the recently TRMC characterization of PCE-10:PCBM blend,[47] both TRMC mobility and carrier lifetime is significantly improved in the all-polymer blend. In addition, we can conclude that P-i-N is a more desirable architecture than BHJ in terms of free charge generation, carrier mobility and diffusion length, resulting in improved carrier collection at the electrodes to achieve high exciton-to-free-carrier yield. The dependence of J_{sc} and V_{oc} on light intensity was measured to examine recombination process in P-i-N and BHJ devices.[48-49] As shown in **Figure 3D**, for

the optimized device, J_{sc} scales almost linearly with light intensity (α=0.98 for both BHJ and P-i-N PBDB-T:N2200 based devices). These values indicate that the charge carrier losses in the all-polymer system are not dominated by bimolecular recombination. Additionally, the V_{oc} of optimal P-i-N devices exhibits a logarithmic dependence on light intensity with a slope of 1.05 kTq^{-1} compared to that of 1.41 kTq^{-1} in BHJ system, indicating less interfacial trap-assisted Shockley-Read-Hall (SRH) recombination. In an ideal P-i-N film, the free electron and hole move more efficiently in single donor and acceptor phase after the exciton dissociation at the interface. In addition, the charge recombination at each electrode could also be reduced in the P-i-N devices due to the improved carrier selectivity.

The higher V_{oc} of P-i-N all-polymer device (0.904 V *vs.* 0.867 V) motivated us to study the energy loss associated with the processes of exciton dissociation and carrier recombination. To get insight into the higher V_{oc} in the P-i-N devices, Fourier transform photocurrent spectroscopy (FTPS) was performed. For organic solar cells, V_{oc} is correlated to the energy of the charge transfer (CT) state (E_{ct}) formed at the donor/acceptor interface. A high V_{oc} requires a high E_{ct} plus a relatively small energy loss. The FTPS data for the solar cells based on P-i-N and bulk PBDB-T:N2200 are shown in **Figure 3E**. Fitting the CT region of the EQE spectra with Equation (2):[50]

$$EQE(E) \propto \frac{1}{E\sqrt{4\pi\lambda kT}} \exp\left\{\frac{-(E_{ct}+\lambda-E)^2}{4\lambda kT}\right\} \quad (1)$$

where k is the Boltzmann's constant, T is the absolute temperature, E_{ct} is the energy of CT states, and λ is related to the width of the CT absorbance band. The E_{ct} values from the fitting are both around 1.40 eV for the P-i-N and BHJ devices. Similar results can be also found from the

electroluminescence measurements (**Figure 3F**). Both devices exhibit similar E_{ct} emission peak at ~950 nm. Non-radiative recombination induced V_{oc} loss [51] was also characterized, which would decrease the V_{oc} by:

$$\Delta V_{oc}^{non\text{-}rad} = -\frac{kT}{q}\ln(EQE_{EL}) \quad (2)$$

where EQE_{EL} is radiative quantum efficiency of the solar cell when charge carriers are injected into the device in the dark. At room temperature, $\Delta V_{oc}^{non\text{-}rad}$ increases by 60 mV when the EQE_{EL} decreases by one order. The EQE_{EL} of the bulk PBDB-T:N2200 device is measured as 4×10^{-5} %, and that of the P-i-N PBDB-T:N2200 blend is 1.6×10^{-4} % (insert in **Figure 3F**). The non-radiative loss for bulk and P-i-N is 0.41 V and 0.38 V, respectively, which corresponds to the V_{oc} difference. The difference in the EQE_{EL} values indicates reduced non-radiative recombination loss in P-i-N system.

In a typical organic solar cell device, the exciton dissociation and charge transport process is strongly affected by the blend morphology. Therefore, a thorough morphological study may be helpful to understand the carrier generation and transport process in all-polymer solar cells. Therefore, we further investigated the all-polymer blend morphology using cross-sectional scanning electron microscopy (SEM), atomic force microscopy (AFM), grazing incidence wide-angle X-ray scattering (GIWAXS),[52] and resonant soft X-ray scattering (RSoXS).[53] Figure S6 shows the cross-sectional SEM analysis of both BHJ and P-i-N film. The BHJ shows quite uniform structure, while the P-i-N film shows different morphological properties. **Figure 4A** shows the AFM topographical images, the neat N2200 film exhibits highly textured surface structure with long range order of polymer fibers, while PBDB-T exhibit amorphous surface

without any fiber structure. When blending highly-crystalline N2200 with amorphous PBDB-T, the relevant bulk blend film exhibits significantly reduced domain order and decreased fiber size, which can well explain the significant decrease in electron mobility of the BHJ relative to the neat N2200. In contrast, when depositing amorphous PBDB-T on top of highly-crystalline N2200, we surprisingly find that the PBDB-T upper layer shows ordered surface structure with polymer fibers. Previous reports have demonstrated that depositing polymer film onto a nano-grooved substrate can further increase the ordering and transport in the polymer thin films.[54] Hence, we believe that the highly ordered N2200 layer can serve as "nano-grooved substrate", which can not only maintain its ordered structure, but also improve the ordering of the upper PBDB-T layer. A similar result is also observed in the GIWAXS measurements (**Figure 4B-4D**). The neat N2200 film is a highly-crystalline film with strong face-on orientation, showing multiple characteristic diffraction peaks in the in-plane direction. The neat PBDB-T film is amorphous with a broad (010) diffraction ring, showing no dominant orientation. In comparison with the BHJ, the P-i-N film exhibits more apparent combined (010) diffraction peaks at ~1.6 $Å^{-1}$ in the near out-of-plane direction, and (100), (001), (200), (300), (002), (400), (003) and (004) peaks at in the in-plane direction respectively, which corresponds to the characteristic scattering peaks of neat N2200. Thus, the combination of surface AFM and GIWAXS characterization indicate that both polymers are highly ordered with favorite orientation, which enables efficient charge separation at interface and better carrier transport within respective phases, as well as increased optical absorption in comparison with the conventional BHJ devices. More detailed information on interfacial phase-separation in the P-i-N was studied via RSoXS. A series of photon energies were used to determine the maximum scattering contrast between the donor and the acceptor polymers (Figure S7). RSoXS likely reflects general phase separation between D/A

materials, and RSoXS from a single component film of polymer likely will have minimal scattering because there is no phase separation.[51] As seen from **Figure 4E**, the PBDB-T:N2200 BHJ shows a relatively sharp scattering peak at ~0.0076 $Å^{-1}$. In contrast, the P-i-N blend film shows a greatly decreased scattering peak at ~0.0076 $Å^{-1}$. Therefore, the BHJ scatters more in RSoXS because there are phase separated D and A regions throughout the entire thickness of the film. For the P-i-N, the only scattering region should come from the burid mixed D/A region at the interface, resulting in a relatively weaker scattering signal.

Finally, in order to understand the charge carrier dynamics in the P-i-N all-polymer solar cells, we mapped the potential difference at the P/N junction interface using Kelvin probe force microscope (KPFM).[55] **Figures 5A-5B** show the morphology and surface potential near the junction of PBDB-T:N2200 bilayer. The set-up for the KPFM measurements is shown in **Figure 5C**, with the drop-casted PBDB-T film covering part of the N2200 layer. The large contrast between junction of PBDB-T and N2200 in **Figure 5B** indicates large Fermi level difference between the two polymers. Following cross-lines at the same position (**Figure 5D**), we find a sharp potential change region in PBDB-T film with ~1μm lateral distance which equal to a ~380 nm film thickness (in height). Likewise, as illustrated in Figure S8-9, we also observe a sharp potential change region of ~400 nm film thicknesses in the N2200 film cast on top of PBDB-T. These potential changes in both PBDB-T and N2200 are caused by the large Fermi level difference between the polymer donor and acceptor, leading to desired electric field distribution near the P/N junction. For organic materials, the free carrier density is relatively low, which results in depletion region longer than the active film thickness in P-i-N all-polymer solar cells. We performed capacitance–voltage (C-V) measurements to investigate their built-in potential (V_{bi}).[56] As shown in Figure S10, The V_{bi} of the P-i-N device is about 0.61 V which is

obviously higher than the 0.52 V for conventional BHJ device. These results are in agreement with the observation in KPFM characterization. These enhanced electric fields are beneficial for driving electrons and holes to transport in separate donor acceptor layer.

The free carrier generation efficiency is a very critical factor when evaluating the P-i-N and BHJ structures. From the photoluminescence (PL) characterization of neat and blend films (Figure S11), both the BHJ and P-i-N all-polymer films exhibit efficient PL quenching. We therefore used ultrafast transient absorption (TA) spectroscopy to further compare exciton dissociation and charge generation efficiency in the BHJ and P-i-N films.[57] When pumped at 400 nm within the strong absorption region of the PBDB-T donor polymer, both films show long-lived large bleaching signals (transmission change $\Delta T/T>0$) with two peaks at 570 nm and 650 nm, as shown in Figure S11a and S11b. In the neat PBDB-T film, the transient bleaching signals with two peaks at 570 nm and 650 nm are also observed (Figure S11c), however, these signals quickly decay at the time scale of 50 picoseconds (ps) as a result of geminate exciton recombination. These results thus indicate that in both BHJ and P-i-N films a significant number of photo-excited excitons diffuse to the D/A interface, and then dissociate to generate charge carriers (polarons) with long lifetime. The hole polarons residing in the PBDB-T deplete the ground state, leading to positive bleaching signals with long lifetime (>500 ps). The hole polarons can also cause the extra absorption at photon energies slightly below the band gap, manifested as the absorption peak centered at ~900 nm in Figure S11a and S11b, whereas this polaron induced peak is absent in the neat donor and acceptor films (see Figure S11c and S11d). To make a quantitative comparison of exciton dissociation and charge transfer, we plot in **Figure 5E** the $\Delta T/T$ dynamics (normalized at 1 ps) probed at 650 nm for the BHJ and P-i-N films, and the neat PBDB-T and N2200 films pumped at 400 nm. The $\Delta T/T$ signals in all films show a

quick rise within 1 ps owing to the photo-generated excitons. But in contrast to the fast decay to nearly zero due to the exciton recombination in the neat films, the ΔT/T in both BHJ and P-i-N films show a fast but small decay within 15 ps and then a very slow recovery longer than 800 ps. The ΔT/T dynamics are very similar for the BHJ and P-i-N films, indicating that the charge transfer rates and efficiencies are comparable in these two films. Actually, similar hole transfers were also observed by selective excitation of N2200 using 800 nm laser pulses (see **Figure 5F**). For both films, the ΔT/T dynamics probed at 650 nm shows an extra rise within 15 ps followed by a very slow decay longer than 800 ps. The extra rise of ΔT/T signal must be due to the dissociation of the excitons at the interface and the consequent formation of hole polarons in PBDB-T. In principle, the BHJ structure has more interfaces than the P-i-N one, thus the exciton diffusion to the interface for charge transfer is more favorable in the BHJ when considering the limited diffusion length before the exciton recombination. But on the contrary, the probability of geminate and bimolecular recombination after exciton dissociation is higher in the BHJ due to its increased and randomly distributed interfaces. Moreover, the intermixed polymer phases in the BHJ show intrinsic difficulty to optimize the side-chain entanglement and backbone orientation between donor and acceptor polymers for efficient charge transfer. These factors overall may result in a similar free carrier generation efficiency in the BHJ and P-i-N films.

We designed and reported efficient all-polymer solar cells with a P-i-N architecture using polymeric donor (PBDB-T) and acceptor (N2200) that delivered a high device efficiency of 9.52 %, which is significantly improved compared to the 6.58 % for conventional PBDB-T:N2200 bulk heterojunction solar cell. A schematic of this P-i-N structure is shown in **Scheme 1**, which consists of highly crystalline and high purity donor and acceptor polymer phases connected by intermixed D/A region to achieve improved charge generation, transport and collection. This P-i-

N structure can also provide enhanced internal electric field and more stable morphology under harsh thermal stress compared with BHJ structure. In addition, long-range exciton from delocalized photoexcitation may enable an immediate probability of charge-transfer over distances, which has been suggested in the previous report.[58] The P-i-N structure can be facilely realized in all-polymer system by manipulating the molecular weight and solubility of the polymers. We further proved the general effect of P-i-N in several other all-polymer systems. Since fine control of the phase-separation morphology in all-polymer BHJ blend remains an intrinsic challenge, the modified P-i-N structure would be extremely advantageous and become a more favorite device structure than dominant BHJ in all-polymer solar cells. We also believe the adoption of P-i-N structure can promote the use of more crystalline conjugated polymers with high carrier mobility.

FIGURES

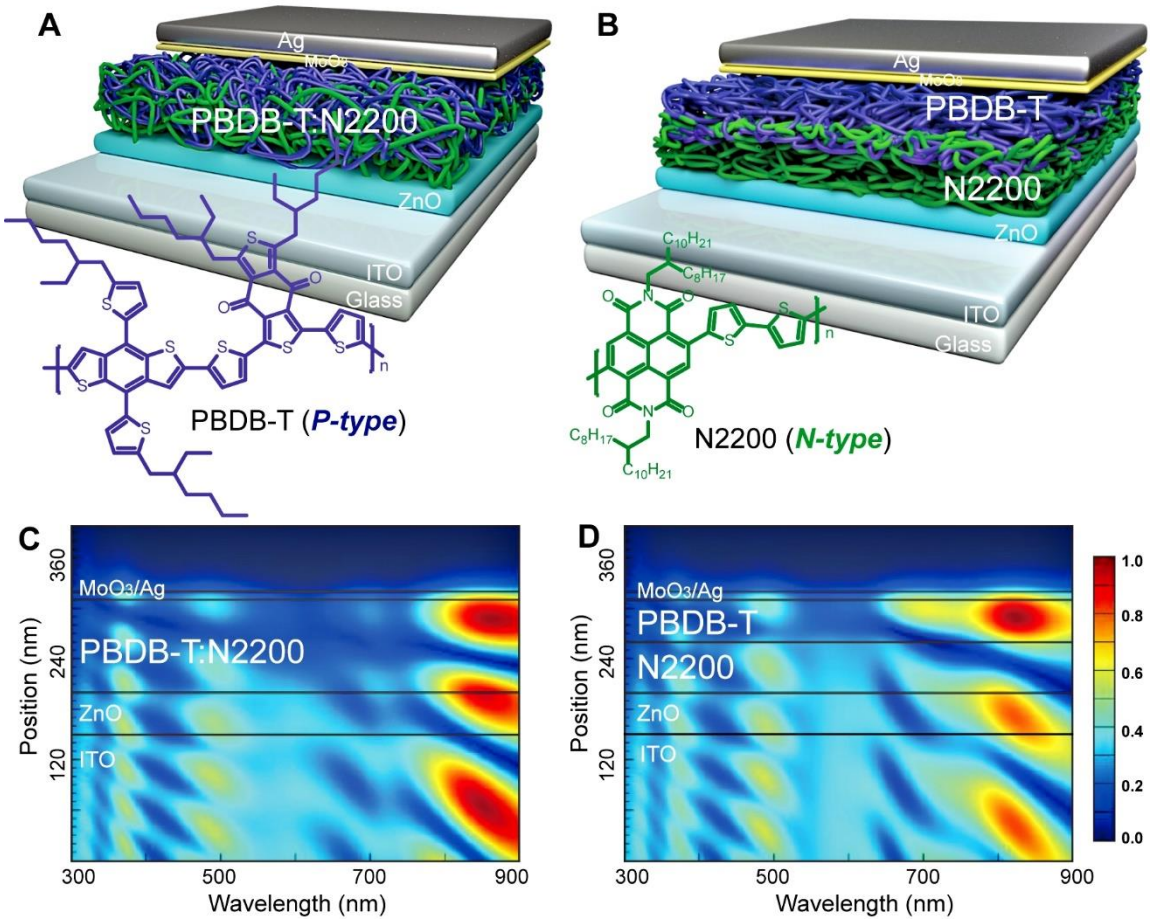

Figure 1. Schematic illustration of the device structure of BHJ (A) and P-i-N (B) all-polymer solar cells together with the chemical structure of PBDB-T and N2200. Optical simulation of photon flux intensity distributions in cross-sectional BHJ (C) and P-i-N (D) all-polymer solar cells. Position 0 nm corresponds to the glass/ITO interface and the P-i-N light source is illuminating from the bottom.

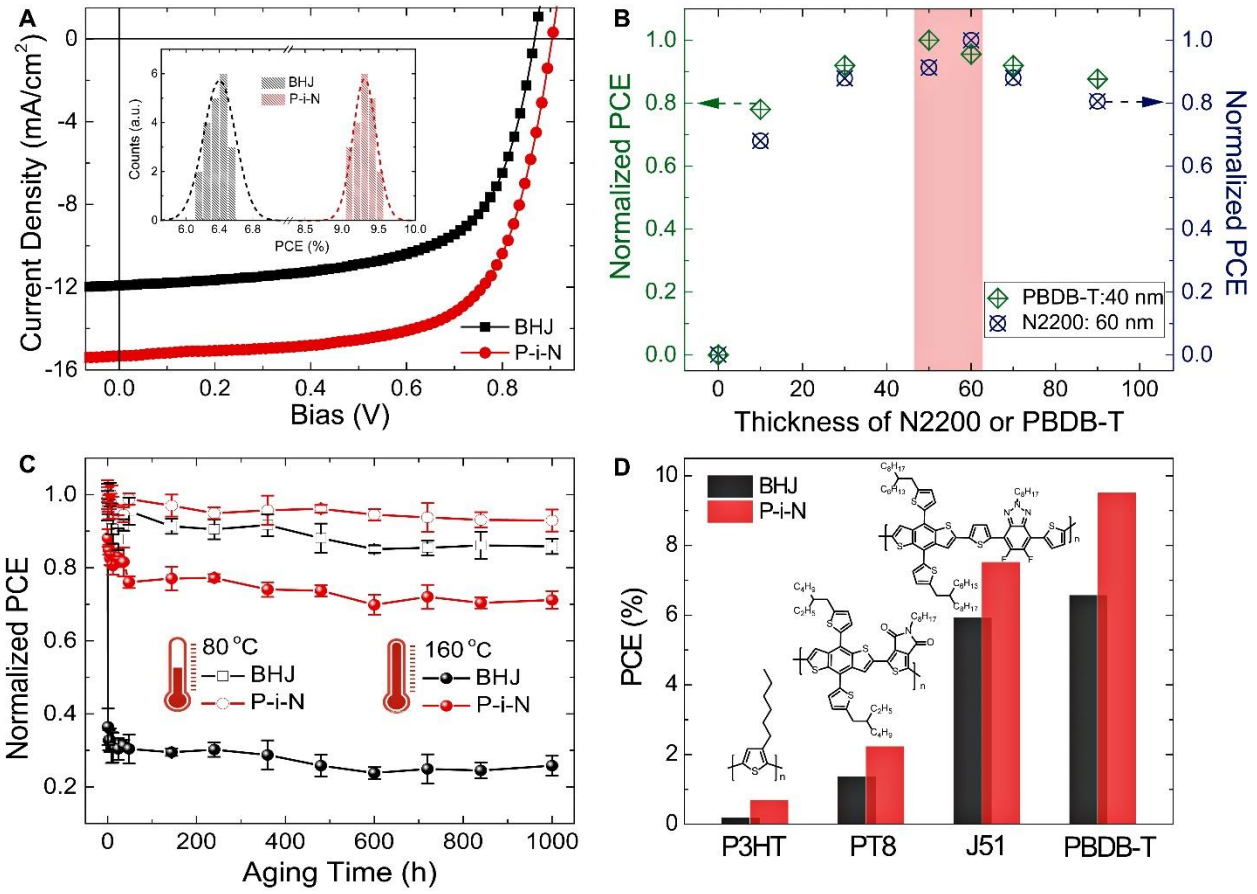

Figure 2. Current–voltage characteristics of optimized BHJ and P-i-N devices under AM 1.5G, 100 mW cm^{-2}, insert is the histogram of the PCE measurements for 20 devices (A). PCEs of P-i-N all-polymer solar cells as a function of N2200 thickness (the thickness of PBDB-T is fixed at 40 nm) or PBDB-T thickness (the thickness of N2200 is fixed at 60 nm) (B). Thermal stability of BHJ and P-i-N all-polymer solar cell devices based on PBDB-T:N2200 kept on the hotplate in N_2-filled glovebox. (C). PCE of all-polymer solar cell based on BHJ and P-i-N structure using P3HT, PT8, J51 and PBDB-T as donor, and N2200 as acceptor (D).

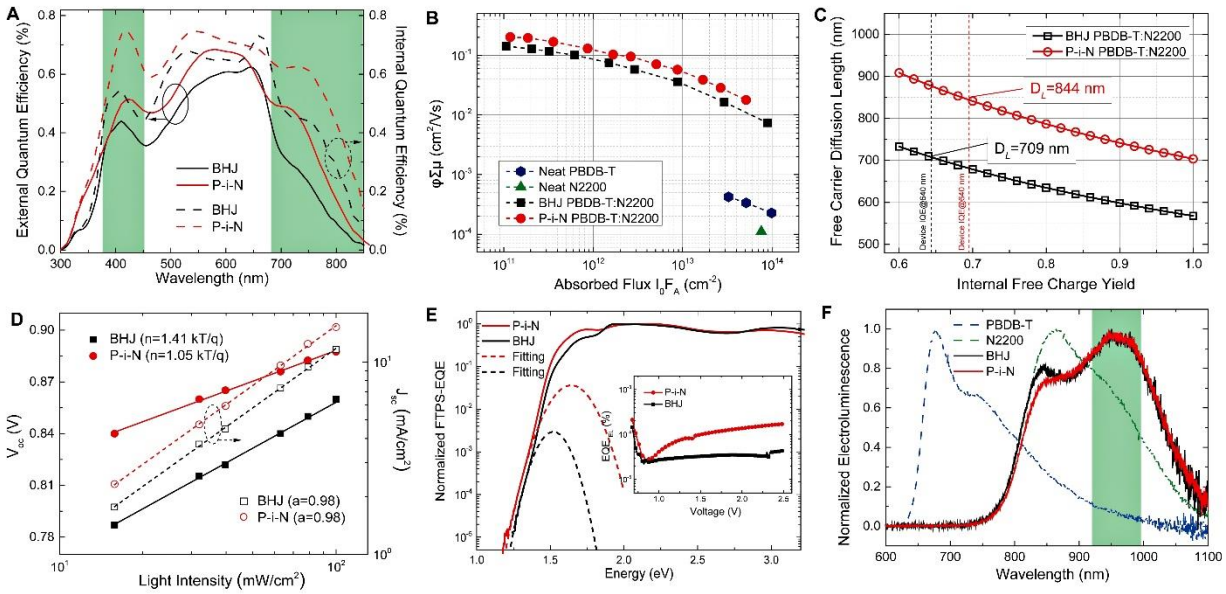

Figure 3. EQE and IQE curves of the optimized BHJ and P-i-N PBDB-T:N2200 solar cells (A). The product of charge carrier yield (ϕ) and sum of free carrier mobilities (Σμ) (B) for BHJ and P-i-N PBDB-T: N2200 blends at a laser excitation wavelength of 640 nm. Calculated free carrier diffusion length as a function of internal free charge yield from TRMC measurements (C). Measurements of J_{SC} and V_{OC} as a function of light intensity (D). FTPS-EQE of BHJ and P-i-N all-polymer devices, insert is the EQE_{EL} of the devices (E). Electroluminescence spectra of devices based on the neat polymers and blend films (F).

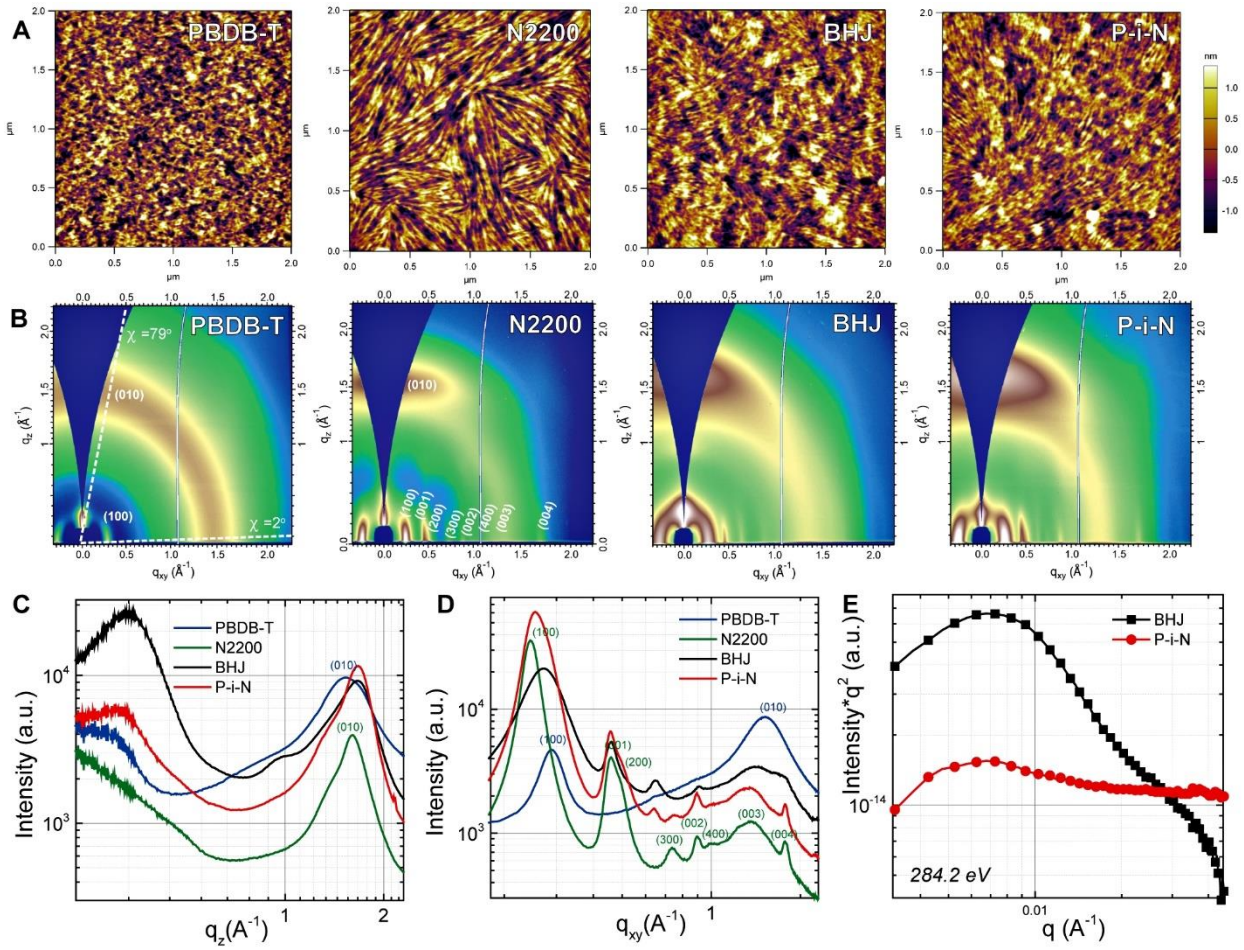

Figure 4. AFM topographical images (A) and GIWAXS two-dimensional diffraction patterns (B) of neat PBDB-T, neat N2200, PBDB-T:N2200 BHJ blend, and PBDB-T on top of N2200 P-i-N blend. Nearly out-of-plane (C) and in-plane (D) of the two-dimensional GIWAXS patterns. RSoXS scattering profiles of the bulk and P-i-N all-polymer blend films using a photon energy of 284.2 eV (E).

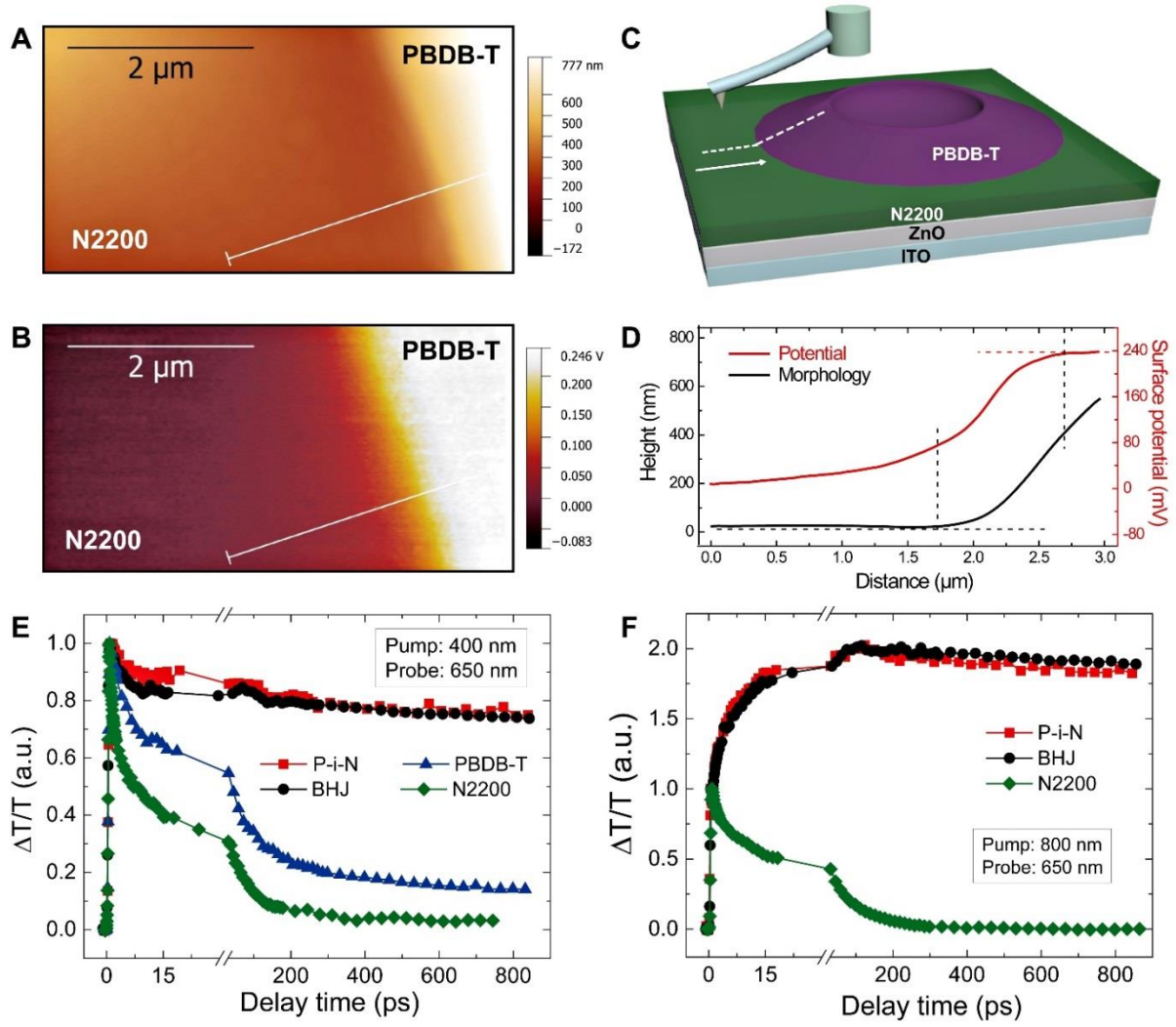

Figure 5. Height morphology (A) and surface potential (B) images of the N2200 layer partially covered by PBDB-T the layer. Illustration of the KPFM measurements (C). Height and surface potential change as a function of scanning distance in N2200 layer partially covered by PBDB-T the layer (D). Comparison of ΔT/T dynamics (normalized at 1 ps) probed at 650 nm in PBDB-T/N2200 BHJ and P-i-N films, and neat PBDB-T and N2200 films under pump excitations of (E) λ=400 nm and (F) λ=800 nm. The pump fluence is I=70 μJ cm^{-2}.

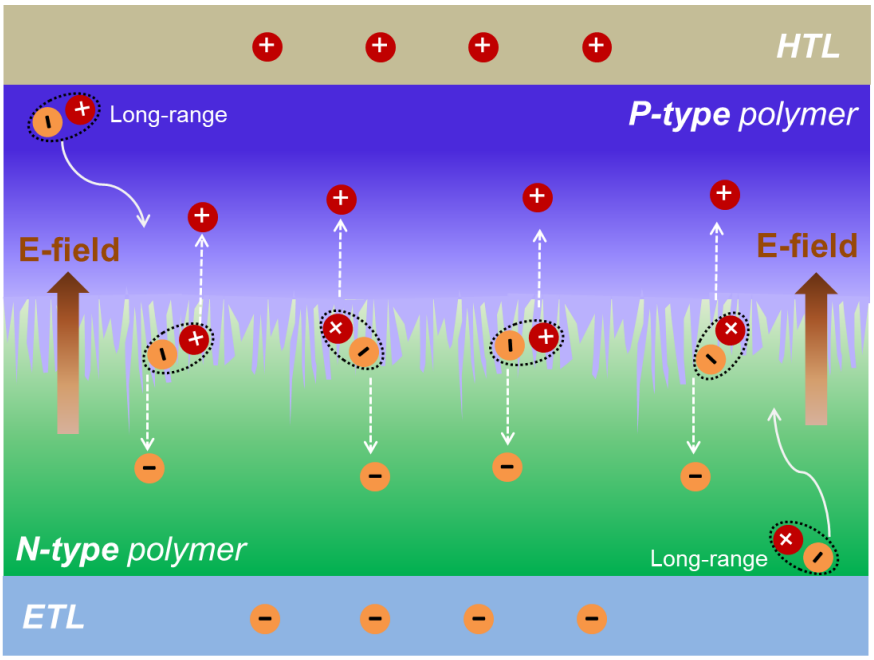

Scheme 1. Illustration of the carrier dynamic in the P-i-N all-polymer blends.

Table 1. Device parameters of BHJ and P-i-N heterojunction all-polymer solar cells.

	V_{oc} (V)	J_{sc} (mA/cm2)	FF (%)	PCE (%)	Yield Mobility Product ($cm^2\ V^{-1}s^{-1}$)	TRMC Lifetime (ns)	E_{loss} (eV)	E_{ct} (eV)	$E^{non\text{-}rad}{}_{loss}$ (eV)
BHJ	0.867 (0.860±0.007)	11.89 (11.27±0.62)	64.4% (61.2±3.2%)	6.58 (6.37±0.21)	0.14	880	0.59	1.41	0.41
P-i-N	0.904 (0.898±0.006)	15.33 (14.79±0.54)	68.7% (66.3±2.4%)	9.52 (9.28±0.24)	0.20	950	0.55	1.40	0.38

ASSOCIATED CONTENT

Supporting Information

Materials and characterizations, device fabrication and measurements, the synthesis of N2200 optical simulation, time-resolved microwave conductivity, FTPS and EQE_{EL} measurement, ultrafast transient absorption measurements, device fabrication of P3HT, PT8 and J51 based solar cells, the preparation of KPFM samples, capacitance-voltage (C-V) measurements, absorption, dark J-V characteristics, cross-sectional SEM images, PL measurements, and the performance parameters of devices optimization. These material are available free of charge via the Internet at http://pubs.acs.org.

Corresponding Author

jyyuan@suda.edu.cn (J. Yuan)

wlma@suda.edu.cn (W. Ma)

Notes

The authors declare no competing financial interest.

ACKNOWLEDGMENT

This work was supported by the Natural Science Foundation of Jiangsu Province of China (BK20170337), the National Natural Science Foundation of China (Grant No. 51803144, 51761145013 and 61674111), and "111" projects. The author thanks the Collaborative Innovation Center of Suzhou Nano Science and Technology, Soochow University, the Priority Academic Program Development of Jiangsu Higher Education Institutions (PAPD). This work was authored in part by the National Renewable Energy Laboratory, operated by Alliance for Sustainable Energy, LLC, for the U.S. Department of Energy (DOE) under Contract No. DE-AC36-08GO28308. BWL acknowledges funding from the Office of Energy Efficiency and

Renewable Energy Solar Energy Technologies Office. The views expressed in the article do not necessarily represent the views of the DOE or the U.S. Government. The U.S. Government retains and the publisher, by accepting the article for publication, acknowledges that the U.S. Government retains a nonexclusive, paid-up, irrevocable, worldwide license to publish or reproduce the published form of this work, or allow others to do so, for U.S. Government purposes.The use of the Advanced Light Source beamline 7.3.3 for grazing incidence wide angle X-ray scattering, beamline 11.0.1.2 for resonant soft X-ray scattering, and beamline 6.3.2 for near edge X-ray absorption fine structure spectroscopy are supported by the Director, Office of Science, Office of Basic Energy Sciences, of the DOE under contract no. DE-AC02-05CH11231.

REFERENCES

(1) Yu, G.; Gao, J.; Hummelen, J. C.; Wudl, F. & Heeger, A. J. Polymer photovoltaic cells:enhanced efficiencies via a network of internal donor-acceptor heterojunctions. *Science* **1995**, *270*, 1789.

(2) Brabec, C. J.; Sariciftci, N. S.; Hummelen, J. C. Plastic solar cells. *Adv. Funct. Mater.* **2001**, *11*, 15.

(3) Cheng, Y.-J.; Yang, S.-H.; Hsu, C.-S. Synthesis of conjugated polymers for organic solar cell applications. *Chem. Rev.* **2009**, *109*, 5868.

(4) Li, Y. F. Molecular design of photovoltaic materials for polymer solar cells: toward suitable electronic energy levels and broad absorption. *Acc. Chem. Res.* **2012**, *45*, 723.

(5) Hsu, B. B.-Y.; Cheng, C.-M.; Luo, C.; Patel, S. N.; Zhong, C.; Sun, H.; Sherman, J.; Lee, B. H.; Ying, L.; Wang, M.; Bazan, G.; Chabinyc, M.; Brédas, J.-L.; Heeger, A. J. The density of states and the transport effective mass in a highly oriented semiconducting polymer: electronic delocalization in 1D. *Adv. Mater.* **2015**, *27*, 7759.

(6) Yao, H.; Ye, L.; Zhang, H.; Li, S.; Zhang, S.; Hou, J. Molecular Design of Benzodithiophene-Based Organic Photovoltaic Materials. *Chem. Rev.* **2016**, *116*, 7397.

(7) Liu, Y.; Zhao, J.; Li, Z.; Mu, C.; Ma, W.; Hu, H.; Jiang, K.; Lin, H.; Ade, H.; Yan, H. Aggregation and morphology control enables multiple cases of high-efficiency polymer solar cells. *Nat. Commun.* **2014**, *5*, 5293.

(8) Hou, J.; Inganäs, O.; Friend, R. H.; Gao, F. Organic Solar Cells Based on Non-fullerene Acceptors. *Nat. Mater.* **2018**, *17*, 119.

(9) Cheng, P.; Li, G.; Zhan, X.; Yang Y. Next-generation organic photovoltaics based on non-fullerene acceptors. *Nat. Photon.* **2018**, *12*, 131.

(10) Zhang, Z.; Tan, H. S.; Guo, X.; Facchetti, A.; Yan, H. Material insights and challenges for non-fullerene organic solar cells based on small molecular acceptors. *Nat. Energy* **2018**, *3*, 720.

(11) Yuan, J.; Zhang, Y.; Zhou, L.; Zhang, G.; Yip, H.-L.; Lau, T.-K.; Lu, X.; Zhu, C.; Peng, H.; Johnson, P. A.; Leclerc, M.; Cao, Y.; Ulanski, J.; Li, Y.; Zou, Y. Single-Junction Organic Solar Cell with over 15% Efficiency Using Fused-Ring Acceptor with Electron-Deficient Core. *Joule* **2019**, *17*, 1140.

(12) Mori, D.; Benten, H.; Okada, I.; Ohkita, H.; Ito, S. Low-bandgap donor/acceptor polymer blend solar cells with efficiency exceeding 4%. *Adv. Energy Mater.* **2014**, *4*, 1301006.

(13) Jung, J. W.; Jo, J. W.; Chueh, C.-C.; Liu, F.; Jo, W. H.; Russell, T. P.; Jen, A. K.-Y. Fluoro-substituted n-type conjugated polymers for additivefree all-polymer bulk heterojunction solar cells with high power conversion efficiency of 6.71%. *Adv. Mater.* **2015**, *27*, 3310.

(14) Hwang, Y.-J.; Earmme, T.; Courtright, B. A. E.; Eberle, F. N.; Jenekhe, S. A. n-Type semiconducting naphthalene diimide-perylene diimide copolymers: controlling crystallinity, blend morphology, and compatibility toward high-performance all-polymer solar cells. *J. Am. Chem. Soc.* **2015**, *137*, 4424.

(15) Li, Z.; Xu, X.; Zhang, W.; Meng, X.; Genene, Z.; Ma, W.; Mammo, W.; Yartsev, A.; Andersson, M. R.; Janssen, R. A. J.; Wang, E. 9.0% power conversion efficiency from ternary all-polymer solar cells. *Energy Environ. Sci.* **2017**, *10*, 2212.

(16) Fan, B.; Ying, L.; Zhu, P.; Pan, F.; Liu, F.; Chen, J.; Huang, F.; Cao, Y. All-polymer solar cells based on a conjugated polymer containing siloxane-functionalized side chains with efficiency over 10%. *Adv. Mater.* **2017**, *29*, 1703906.

(17) Yuan, J.; Ford, M. J.; Xu, Y.; Zhang, Y.; Bazan, G. C.; Ma, W. Improved tandem all-polymer solar cells performance by using spectrally matched subcells. *Adv. Energy Mater.* **2018**, *8*, 1703291.

(18) Facchetti, A. Polymer donor-polymer acceptor (all-polymer) solar cells. *Mater. Today* **2013**, *16*, 123.

(19) Kim, T.; Kim, J. H.; Kang, T. E.; Lee, C.; Kang, H.; Shin, M.; Wang, C.; Ma, B.; Jeong, U.; Kim, T. S.; Kim, B. J. Flexible, highly efficient all-polymer solar cells. *Nat. Commun.* **2015**, *6*, 8547.

(20) Zhang, Y.; Xu, Y.; Ford, M. J.; Li, F.; Sun, J.; Ling, X.; Wang, Y.; Gu, J.; Yuan, J.; Ma, W. Thermally stable all-polymer solar cells with high tolerance on blend ratios. *Adv. Energy Mater.*, **2018**, *8*, 1800029.

(21) Zhou, E.; Cong, J.; Hashimoto, K.; Tajima, K. Control of miscibility and aggregation via the material design and coating process for high-performance polymer blend solar cells. *Adv. Mater.* **2013**, *25*, 6991.

(22) Mori, D.; Benten, H.; Okada, I.; Ohkita, H.; Ito, S. Highly efficient charge carrier generation and collection in polymer/polymer blend solar cells with a power conversion efficiency of 5.7%. *Energy Environ. Sci.* **2014**, *7*, 2939.

(23) Kang, H.; Uddin, M. A.; Lee, C.; Kim, K.-H.; Nguyen, T. L.; Lee, W.; Li, Y.; Wang, C.; Woo, H. Y.; Kim, B. J. Determining the role of polymer molecular weight for high-performance all-polymer solar cells: its effect on polymer aggregation and phase separation. *J. Am. Chem. Soc.* **2015**, *137*, 2359.

(24) Li, Z.; Xu, X.; Zhang, W.; Meng, X.; Ma, W.; Yartsev, A.; Inganas, O.; Andersson, M. R.; Janssen, R. A.; Wang, E. High performance all-polymer solar cells by synergistic effects of fine-tuned crystallinity and solvent annealing. *J. Am. Chem. Soc.* **2016**, *138*, 10935.

(25) Mu, C.; Liu, P.; Ma, W.; Jiang, K.; Zhao, J.; Zhang, K.; Chen, Z.; Wei, Z.; Yi, Y.; Wang, J.; Yang, S.; Huang, F.; Facchetti, A.; Ade, H.; Yan, H. High-efficiency all-Polymer solar cells based on a pair of crystalline low-bandgap polymers. *Adv. Mater.* **2014**, *26*, 7224.

(26) Schubert, M.; Collins, B. A.; Mangold, H.; Howard, I. A.; Schindler, W.; Vandewal, K.; Roland, S.; Behrends, J.; Kraffert, F.; Steyrleuthner, R.; Chen, Z.; Fostiropoulos, K.; Bittl, R.; Salleo, A.; Facchetti, A.; Laquai, F.; Ade, H. W.; Neher, D. Correlated

donor/acceptor crystal orientation controls photocurrent generation in all-polymer solar cells. *Adv. Funct. Mater.* **2014**, *24*, 4068.

(27) Yuan, J.; Guo, W.; Xia, Y.; Ford, M. J.; Jin, F.; Liu, D.; Zhao, H.; Inganäs, O.; Bazan, G. C.; Ma, W. Comparing the Device Physics, Dynamics and Morphology of Polymer Solar Cells Employing Conventional PCBM and Non-Fullerene Polymer Acceptor N2200. *Nano Energy* **2017**, *35*, 251.

(28) Yip, H.-L.; Jen, A. K. Y. Recent advances in solution-processed interfacial materials for efficient and stable polymer solar cells. *Energy Environ. Sci.* **2012**, *5*, 5994.

(29) Huang, Y.; Kramer, E. J.; Heeger, A. J.; Bazan G. C. Bulk heterojunction solar cells: morphology and performance relationships. Chem. Rev. **2014**, *114*, 7006.

(30) Tang, C. W. Two-layer organic photovoltaic cell. *Appl. Phys. Lett.* **1986**, *48*, 183.

(31) Wang, D. H.; Moon, J. S.; Seifter, J.; Jo, J.; Park, J. H.; Park, O. O.; Heeger, A. J. Sequential processing: control of nanomorphology in bulk heterojunction solar cells. *Nano Lett.* **2011**, *11*, 3163.

(32) Zhang, G.; Huber, R. C.; Ferreira, A. S.; Boyd, S. D.; Luscombe, C. K.; Tolbert, S. H.; Schwartz, B. J. Crystallinity effects in sequentially processed and blend-cast bulk heterojunction polymer/fullerene photovoltaics. *J. Phys. Chem. C* **2014**, *118*, 18424.

(33) Yao, K.; Intemann, J. J.; Yip, H.-L.; Liang, P.-W.; Chang, C.-Y.; Zang, Y.; Li, Z.; Chen Y.; Jen, A. K.-Y. Efficient all polymer solar cells from layer-evolved processing of a bilayer inverted structure. *J. Mater. Chem. C* **2014**, *2*, 416.

(34) Cui, Y.; Zhang, S.; Liang, N.; Kong, J.; Yang, C.; Yao, H.; Ma, L.; Hou, J. Toward efficient polymer solar cells processed by a solution-processed layer-by-layer approach. *Adv. Mater.* **2018**, *30*, 1802499.

(35) Sun, R.; Guo, J.; Sun, C.; Wang, T.; Luo, Z.; Zhang, Z.; Jiao, X.; Tang, W.; Yang, C.; Li, Y.; Min J. A universal layer-by-layer solution-processing approach for efficient non-fullerene organic solar cells. *Energy Environ. Sci.* **2019**, 12, 384.

(36) Yan, H.; Chen, Z.; Zheng, Y.; Newman, C.; Quinn, J. R.; Dotz, F.; Kastler, M.; Facchetti, A. A high-mobility electron-transporting polymer for printed transistors. *Nature* **2009**, *457*, 679.

(37) Steyrleuthner, R.; Di Pietro, R.; Collins, B. A.; Polzer, F.; Himmelberger, S.; Schubert, M.; Chen, Z.; Zhang, S.; Salleo, A.; Ade, H.; Facchetti, A.; Neher, D. The role of

regioregularity, crystallinity, and chain orientation on electron transport in a high-mobility n-type copolymer. *J. Am. Chem. Soc.* **2014**, *136*, 4245.

(38) Shi, S.; Yuan, J.; Ding, G.; Ford, M.; Lu, K.; Shi, G.; Sun, J.; Ling, X.; Li, Y.; Ma, W. Improved all-polymer solar cell performance by using matched polymer acceptor. *Adv. Funct. Mater.* **2016**, *26*, 5669.

(39) Chen, J.-D.; Li, Y.-Q.; Zhu, J.; Zhang, Q.; Xu, R.-P.; Li, C.; Zhang, Y.-X.; Huang, J.-S.; Zhan, X.; You, W.; Tang, J.-X. Polymer solar cells with 90% external quantum efficiency featuring an ideal light-and charge-manipulation layer. *Adv. Mater.* **2018**, *30*, 1706083.

(40) Erb, T.; Zhokhavets, U.; Gobsch, G.; Raleva, S.; Stühn, B.; Schilinsky, P.; Waldauf, C.; Brabec, C. J. Correlation between structural and optical properties of composite polymer/fullerene film for organic solar cells. *Adv. Funct. Mater.* **2005**, *15*, 1193.

(41) Ye, L.; Jiao, X.; Zhou, M.; Zhang, S.; Yao, H.; Zhao, W.; Xia, A.; Ade, H.; Hou, J. Manipulating aggregation and molecular orientation in all-polymer photovoltaic cells. *Adv. Mater.* **2015**, *27*, 6046.

(42) Xu, Y.; Yuan, J.; Sun, J.; Zhang, Y.; Ling, X.; Wu, H.; Zhang, G.; Chen, J.; Wang, Y.; Ma, W. Widely applicable n-Type molecular doping for enhanced photovoltaic performance of all-polymer solar cells. *ACS Appl. Mater. Interfaces*, **2018**, *10*, 2776.

(43)Liu, X.; Zou, Y.; Wang, H.-Q.; Wang, L.; Fang, J.; Yang, C. High-performance All-polymer solar cells with a high fill factor and a broad tolerance to the Donor/Acceptor ratio. *ACS Appl. Mater. Interfaces* **2018**, *10*, 38302.

(44) Shi, G.; Yuan, J.; Huang, X.; Lu, Y.; Liu, Z.,; Peng, J.; Ding, G.; Shi, S.; Sun, J.; Lu, K.; Wang, H.-Q.; Ma, W. Combinative effect of additive and thermal annealing processes delivers high efficiency all-polymer solar cells. *J. Phys. Chem. C* **2016**, *119*, 25298.

(45) Yuan, J.; Xu, Y.; Shi, G.; Ling, X.; Ying, L.; Huang, F.; Lee, T. H.; Woo, H. Y.; Kim, J. Y.; Cao, Y.; Ma, W. Engineering the morphology via processing additives in multiple all-polymer solar cells for improved performance. *J. Mater. Chem. A* **2018**, *6*, 10421.

(46) Gao, L.; Zhang, Z.-G.; Xue, L.; Min, J.; Zhang, J.; Wei, Z.; Li, Y. All-polymer solar cells based on absorption-complementary polymer donor and acceptor with high power conversion efficiency of 8.27%. *Adv. Mater.*, **2016**, *28*, 1884.

(47)Garner, L. E.; Bera, A.; Larson, B. W.; Ostrowski, D. P.; Pal A. J.; Braunecker, W. A.

Promoting morphology with a favorable density of states using diiodooctane to improve organic photovoltaic device efficiency and charge carrier lifetimes. *ACS Energy Lett.* **2017**, *2*, 1556.

(48) Koster, L. J. A.; Mihailetchi, V. D.; Xie, H.; Blom, P. W. M. Origin of the light intensity dependence of the short-circuit current of polymer/fullerene solar cells. *Appl. Phys. Lett.* **2005**, *87*, 203502.

(49) Koster, L. J. A.; Mihailetchi, V. D. Ramaker, R.; Blom, P. W. M. Light intensity dependence of open-circuit voltage of polymer:fullerene solar cells. *Appl. Phys. Lett.* **2005**, *86*, 123509.

(50) Vandewal, K.; Tvingstedt, K.; Gadisa, A.; Inganäs, O.; Manca, J. V. On the origin of the open-circuit voltage of polymer-fullerene solar cells. *Nat. Mater.* **2009**, *8*, 904.

(51) Yao, J.; Kirchartz, T.; Vezie, M. S.; Faist, M. A.; Gong, W.; He, Z.; Wu, H.; Troughton, J.; Watson, T.; Bryant, D.; Nelson, J. Quantifying losses in open-circuit voltage in solution-processable solar cells. J. *Phys. Rev. Applied* **2015**, *4*, 014020.

(52) Rivnay, J.; Mannsfeld, S. C. B.; Miller, C. E.; Salleo, A.; Toney, M. F. Quantitative determination of organic semiconductor microstructure from the molecular to device scale. *Chem. Rev.* **2012**, *112*, 5488.

(53) Collins, B. A.; Cochran, J. E.; Yan, H.; Gann, E.; Hub, C.; Fink, R.; Wang, C.; Schuettfort, T.; McNeill, C. R.; Chabinyc, M. L.; Ade, H. Polarized X-ray scattering reveals non-crystalline orientational ordering in organic films. *Nat. Mater.* **2012**, *11*, 536.

(54) Tseng, H.-R.; Phan, H.; Luo, C.; Wang, M.; Perez, L. A.; Patel, S. N.; Ying, L.; Kramer, E. J.; Nguyen, T.-Q.; Bazan, G. C.; Heeger, A. J. High-mobility field-effect transistors fabricated with macroscopic aligned semiconducting polymers. *Adv. Mater.* **2014**, *26*, 2993.

(55) Chen, Q.; Mao, L.; Li, Y.; Kong, T.; Wu, N.; Ma, C.; Bai, S.; Jin, Y.; Wu, D.; Lu, W.; Wang, B.; Chen, L. Quantitative operando visualization of the energy band depth profile in solar cells. *Nat. Commun.* **2015**, *6*, 7745.

(56) Sun, Y.; Liu, Z.; Yuan, J.; Chen, J.; Zhou, Y.; Huang, X.; Ma, W. Polymer selection toward efficient polymer/PbSe planar heterojunction hybrid solar cells. *Org. Electron.* **2015**, *24*, 263.

(57) Jin, F.; Yuan, J.; Guo, W.; Xu, Y.; Zhang, Y.; Sheng, C.; Ma, W.; Zhao, H. Improved charge generation via ultrafast effective hole-transfer in all-polymer photovoltaic blends with large highest occupied molecular orbital (HOMO) energy offset and proper crystal orientation. *Adv. Funct. Mater.* **2018**, *28*, 1801611.

(58) Kaake, L. G.; Moses, D.; Heeger, A. J. Coherence and uncertainty in nanostructured organic photovoltaics. *J. Phys. Chem. Lett.* **2013**, *4*, 2264.